Received: 22 June 2023 | Revised: 7 July 2023 | Accepted: 22 August 2023

DOI: 10.1002/pamm.202300030

RESEARCH ARTICLE

Numerical investigation of mixed convection flow over a heated horizontal plate of finite length

Lukas Babor

Institute of Fluid Mechanics and Heat Transfer, TU Wien, Vienna, Austria

Correspondence
Lukas Babor, Institute of Fluid Mechanics and Heat Transfer, TU Wien, Getreidemarkt 9, 1060 Vienna, Austria.
Email: lukas.babor@tuwien.ac.at

Funding information
AIC Androsch International Management Consulting GmbH

Abstract

The present numerical study concerns the steady two-dimensional laminar mixed convection flow of Newtonian fluid over a heated horizontal plate of finite length at a zero angle of attack for large Peclet and small Prandtl and Richardson numbers. The plate is located in a horizontal channel of finite height. Buoyancy induces a uniform hydrostatic pressure jump at the trailing edge and across the thermal wake, which is compensated by a perturbation of the outer potential flow according to the Kutta condition. Counter-intuitively, the total lift force acting on the plate points in the opposite direction compared to the buoyancy force. The numerical solution obtained with the Finite Element solver FEniCS is compared to an analytical boundary-layer solution from the literature. For small values of the Richardson number (Ri), an excellent agreement between the numerical and analytical solutions is observed. When Ri exceeds a certain threshold, the flow separates near the leading edge at the lower side of the plate. For some narrow intervals of Ri, three co-existing solutions of the governing equations are found, which differ by the size of the separation bubble. The flow separation can be suppressed by bending the leading edge.

1 | PROBLEM DESCRIPTION

Consider a horizontal plate (red in Figure 1) of finite length L and uniform temperature T_p in an incoming flow at a zero angle of attack with a uniform far-field velocity $\vec{u}_\infty$ and temperature $T_\infty < T_p$. Viscous and thermal boundary layers develop along both the lower and the upper sides of the plate. In the absence of gravity and for large Peclet (Pe_L) and Reynolds (Re_L) numbers, the boundary layers are at the leading order self-similar and identical to a flow around a semi-infinite plate extending to downstream infinity, since the trailing edge does not have a significant upstream influence. The velocity in the viscous boundary layer then follows the famous solution of Blasius [1] and for some (limiting) values of the Prandtl number $\mathrm{Pr} = \mathrm{Pe}_L/\mathrm{Re}_L$, analytical solutions for the temperature across the thermal boundary layer exist as well (see, e.g., pp. 215–219 of [2]). The present work studies numerically the effect of weak buoyancy, quantified by the Richardson number (Ri), on the flow of small Prandtl number fluid, $\mathrm{Pr} \ll 1$, for which analytical results are available in the literature [3–5]. The low-Prandtl-number limit is applicable to liquid metals with $\mathrm{Pr} \sim \mathcal{O}(10^{-2})$, which are of interest for their unique chemical and electric properties [6]. In this limit, the thermal boundary layer is inviscid, while the viscous effects are restricted to a thin viscous sub-layer. It is expected that some of the fundamental phenomena described here will also qualitatively apply to the flow of air with $\mathrm{Pr} = 0.7$.

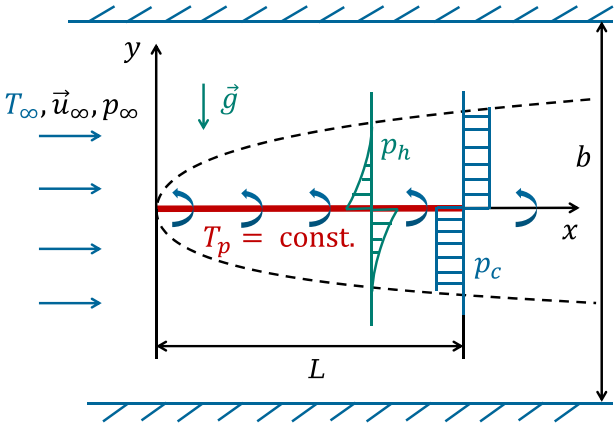

FIGURE 1 Sketch of the problem. The heated plate is shown in red. The dashed line illustrates the edge of the thermal boundary layer. The anti-clockwise curved arrows indicate the perturbation of the outer potential flow, on which the plate and the wake act as a potential vortex sheet. p_h and p_c are the deviation of the hydrostatic pressure from p_∞ and the pressure induced by the outer flow, respectively.

The buoyancy force acts in the vertical direction, perpendicular to the horizontal plate. Since the vertical velocity vanishes at the impermeable plate surface, the buoyancy force in the thermal boundary layer does not directly induce vertical acceleration, but it is compensated by a perturbation of the hydrostatic pressure (pp. 281–289 of [2]), illustrated as p_h in Figure 1. As the thickness of the thermal boundary layer grows, the deviation from the far-field pressure also increases in the streamwise direction. This leads to a horizontal pressure gradient within the thermal boundary layer. In the case of a semi-infinite heated plate, the favorable pressure gradient at the upper side of the plate induces flow acceleration, while the adverse pressure gradient decelerates the flow at the lower side of the plate according to the Bernoulli equation.

Although such *indirect* mixed convection over a semi-infinite horizontal plate has been studied in the literature (see, e.g., pp. 288–289 of [2] for a survey), Schneider [3] realized that in the more practical case of a finite plate, the flow differs substantially. The hydrostatic pressure jump at the trailing edge is compensated by an induced circulation in the outer potential flow to satisfy the Kutta condition. From the point of view of the outer flow, the plate acts as a potential vortex sheet (illustrated by the curved arrows in Figure 1). This is similar to the classical aerodynamics problem of a forced flow around a plate at a non-zero angle of attack. The outer flow imposes an additional pressure p_c (illustrated in Figure 1) onto the boundary layer, which in the present case of a finite horizontal heated plate compensates the hydrostatic pressure jump at the trailing edge and in the wake.

Across the wake, the hydrostatic pressure jump is constant. Thus, the wake contributes to the induced outer flow as a vortex distribution of uniform strength. This influence of the wake, which causes the main difference compared to the classical flow around an adiabatic plate at a non-zero angle of attack, presents a severe complication of the present problem. As the wake extends to downstream infinity, it induces an infinite perturbation of the outer flow. A finite flow solution requires some additional outer boundary condition. In the original analysis [3], Schneider introduces a flow straightener, at which the vertical velocity vanishes, at a large but finite distance upstream of the plate. In the subsequent paper [4], the plate is instead located in a channel, the height of which $b \to \infty$ as the buoyancy parameter $\mathrm{Ri} \to 0$. Müllner and Schneider [5] generalize the analytical flow solution to a plate in a channel of an arbitrary height. Savić and Steinrück [7] obtain a finite solution for the flow around the plate by introducing a positive angle of attack with respect to the far-field velocity, instead of the additional outer boundary conditions. They show that the upward deflection and acceleration of the wake by buoyancy leads to a decaying strength of the induced potential vortex distribution with the distance from the trailing edge, at the expense of an unbounded velocity in the far wake.

The analytical solutions [3–5] for large Peclet and small Prandtl and Richardson numbers show that the effect of buoyancy on the flow around a finite plate is typically opposite compared to the flow around a semi-infinite plate. In the former case, the total lift force acting on the plate is directed opposite to the buoyancy force. This is linked to an overall acceleration (deceleration) of the outer flow at the lower (upper) side of the plate by the induced anti-clockwise circulation. Furthermore, the circulation leads to nose suction as for plates at a non-zero angle of attack.

This work compares the numerical solution of the steady two-dimensional Navier–Stokes equations to the analytical solution of Müllner and Schneider [5] using equivalent boundary conditions (Figure 1) and compatible parameters $\mathrm{Pe}_L \gg 1$, $\mathrm{Pr} \ll 1$, and $\mathrm{Ri} \ll 1$. The complete formulation of the problem and the numerical solution methods are provided in Sections 2 and 3. Section 4 shows an excellent agreement between the numerical and analytical solutions for sufficiently

low Richardson number. Section 4.1 addresses flow separation near the leading edge when the Richardson number exceeds a certain threshold and a non-uniqueness of the flow in certain intervals of the Richardson number. Section 4.2 shows that the separation can be avoided, for example, by bending the leading edge. The results and planned extensions of this work are summarized in Section 5.

2 | PROBLEM FORMULATION

For the purpose of the present numerical study, a thin horizontal plate of length L and thickness $d = 10^{-3}L$ is considered with the leading and the trailing edges rounded with a constant radius of curvature. The plate is located at the mid-height of a horizontal channel. The channel heights b of 10 L and 20 L are considered. The distance between the channel inlet and the leading edge of the plate is 30 L. This distance is sufficiently large such that the induced perturbation of the potential flow can be neglected at the inlet, but sufficiently small such that the viscous boundary layers at the channel walls remain thin relative to the channel height at the streamwise position of the plate. The channel continues to infinity in the downstream direction. The continuation of the channel far behind the plate will be modeled with appropriate outflow boundary condition.

The Cartesian coordinate system, sketched in Figure 1, originates at the tip of the leading edge, with x-coordinate in the plane of the plate and y-coordinate perpendicular to the plate. Dimensionless coordinates, velocities, and deviations from the far field pressure and temperature

$$(X,Y) = \frac{(x,y)}{L}, \qquad \vec{U} = (U,V) = \frac{(u,v)}{u_\infty}, \qquad P = \frac{p-p_\infty}{\rho u_\infty^2}, \qquad \theta = \frac{T-T_\infty}{T_p - T_\infty}, \tag{1}$$

will be employed, referred to the plate length L, the incoming velocity u_∞, twice the stagnation pressure ρu_∞^2, where ρ is the fluid density, and the temperature difference between the plate and the incoming flow $\Delta T = T_p - T_\infty$. The Boussinesq approximation is utilized, that is, the flow is modeled as incompressible and the effects of buoyancy are reduced to a bulk force term in the vertical momentum balance. The scaled steady two-dimensional flow is then governed by the Navier–Stokes and energy equations in dimensionless form

$$\left(\vec{U}\cdot\vec{\nabla}\right)\vec{U} = -\vec{\nabla}P + \frac{\mathrm{Pr}}{\mathrm{Pe}_L}\vec{\nabla}\cdot\left(\vec{\nabla}\vec{U} + \vec{\nabla}\vec{U}^{\mathrm{T}}\right) + \frac{\sqrt{\pi}}{4}\sqrt{\mathrm{Pe}_L}\,\mathrm{Ri}\,\theta\,\vec{e}_y, \tag{2}$$

$$\vec{\nabla}\cdot\vec{U} = 0, \tag{3}$$

$$\vec{U}\cdot\vec{\nabla}\theta = \frac{1}{\mathrm{Pe}_L}\Delta\theta, \tag{4}$$

together with boundary conditions. The governing parameters are the Prandtl number $\mathrm{Pr} = \nu/\kappa$, the Peclet number based on the plate length $\mathrm{Pe}_L = u_\infty L/\kappa$, and the Richardson number $\mathrm{Ri} = 4g\beta\Delta T\sqrt{\kappa L}/\sqrt{\pi u_\infty^5}$, where ν, κ, g, and β are the kinematic viscosity, heat diffusivity, acceleration of gravity and thermal expansion coefficient, respectively. In this work, the values of $\mathrm{Pr} = 0.02$ and $\mathrm{Pe}_L = 400$ are fixed and the effect of Ri on the flow is studied.

At the plate surface, no-slip, no-penetration and uniform temperature are prescribed

$$\vec{U} = 0,\ \theta = 1 \quad \text{at } Y = \begin{cases} \pm\sqrt{(D/2)^2 - (X - D/2)^2} & \text{for } 0 \le X < D/2 \\ \pm D/2 & \text{for } D/2 \le X \le 1 - D/2, \\ \pm\sqrt{(D/2)^2 - (X - 1 + D/2)^2} & \text{for } 1 - D/2 < X \le 1 \end{cases} \tag{5}$$

where $D = d/L = 10^{-3}$ is the dimensionless plate thickness. The no-slip, no-penetration channel walls are adiabatic

$$\vec{U} = 0,\ \frac{\partial\theta}{\partial Y} = 0 \quad \text{at } Y = \pm\frac{B}{2}, \tag{6}$$

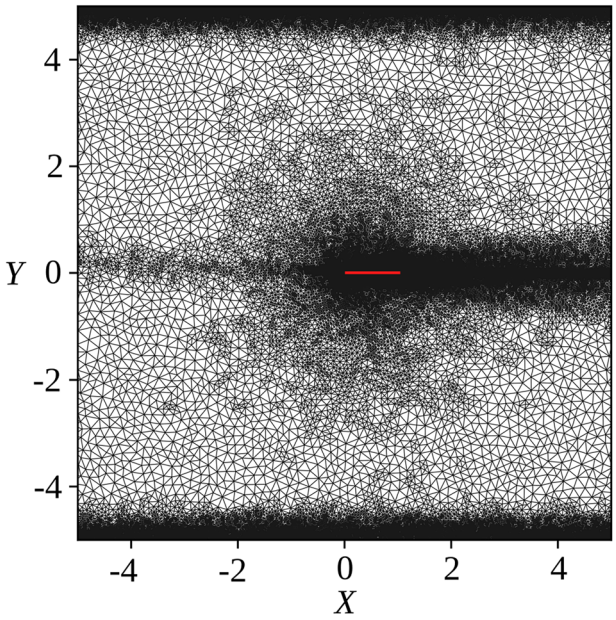

FIGURE 2 Section of the adaptively refined mesh for $B = 10$. The plate is indicated by the red line. The inflow and outflow sections of the channel are trimmed.

where $B = b/L$ is the dimensionless channel height. The far-field velocity and temperature are prescribed at the inlet of the channel

$$\vec{U} = \vec{e}_x,\ \theta = 0 \quad \text{at } X = -30. \tag{7}$$

At the distance of 30 plate lengths behind the plate trailing edge, the continuation of the channel is approximated with the homogeneous Neumann condition for temperature, free slip, and hydrostatic pressure (depending on temperature) acting in the normal direction $\vec{n} = \vec{e}_x$ to an artificial vertical outflow boundary

$$\left.\begin{aligned} \left[\frac{\mathrm{Pr}}{\mathrm{Pe}_L}\left(\vec{\nabla}\vec{U} + \vec{\nabla}\vec{U}^{\mathrm{T}}\right) - P\mathbf{I}\right]\cdot\vec{n} &= \frac{\sqrt{\pi}}{4}\sqrt{\mathrm{Pe}_L}\,\mathrm{Ri}\,\vec{n}\int_{-B/2}^{Y}\theta(\bar{Y})\mathrm{d}\bar{Y}, \\ \vec{n}\cdot\vec{\nabla}\theta &= 0 \end{aligned}\right\} \quad \text{at } X = 31. \tag{8}$$

It was confirmed by numerical experimentation that the distance is sufficient such that the flow around the plate is independent of the position of the outflow boundary.

3 | NUMERICAL METHODS

The numerical solution is computed with the Finite Element solver FEniCS. To that end, the computational domain is discretized into an unstructured triangular mesh. The leading and trailing edges are discretized into 50 line segments each. An initial coarse mesh is generated with the FEniCS module `mshr`, setting the global resolution parameter to $N = 200$. The minimum number of elements along each side of the plate is set to 100. Afterward, the mesh is refined with the Goal-Oriented Adaptive Mesh Refinement algorithm. The total force acting on the plate is employed as the refinement goal, with the relative tolerance of 10^{-4}. A section of the final mesh is shown in Figure 2. It is strongly refined at the channel walls, around the plate, and in the wake.

The governing equations (2–4) are discretized with the continuous Galerkin method. Namely, the Navier–Stokes subsystem (2, 3) is discretized with the 3rd order Taylor–Hood elements, where the velocity and pressure are approximated with 3rd and 2nd order elementwise polynomials, respectively. Temperature is discretized with the same polynomial basis as velocity. The resulting non-linear system of equations is solved with the Newton method.

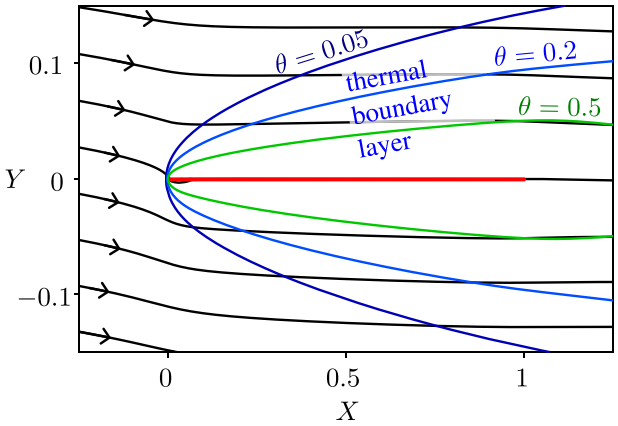

FIGURE 3 Streamlines (black) and isotherms (blue and green) near the plate (red) for Ri = 0.05 and $B = 20$.

For simplicity, the integral relationship (8) between pressure and temperature at the outflow boundary was enforced iteratively with an additional outer loop. The computation is started with the standard *zero-stress* outflow condition

$$\left[\frac{\mathrm{Pr}}{\mathrm{Pe}_L}\left(\vec{\nabla}\vec{U} + \vec{\nabla}\vec{U}^{\mathrm{T}}\right) - P\mathbf{I}\right]\cdot\vec{n} = \vec{0} \quad \text{at } X = 31, \tag{9}$$

to obtain the initial temperature profile along the outflow boundary. The outflow pressure profile is then prescribed according to (8), and a new solution is computed. The iterations are repeated until the outflow profiles converge to the relative tolerance of 10^{-5}.

4 | RESULTS

The flow near the plate for $B = 20$ and Ri = 0.05 is visualized by streamlines in Figure 3. The induced counter-clockwise circulation in the outer flow manifests itself by a downward velocity component upstream of the plate. A very small separation bubble is visible near the leading edge at the lower side of the plate. As the streamlines are vertically compressed (stretched) below (above) the plate, the velocity is higher (lower) relative to the inlet velocity. Qualitatively, the effect of buoyancy on the flow is opposite as compared to the case of a semi-infinite plate, for which the velocity above the plate would be higher than below the plate.

The difference between the flows around a finite and semi-infinite plate is also clearly illustrated by the pressure distribution acting on the plate surface. For simplicity, only the (dimensionless deviation from the far-field) pressure along the upper side of the plate is shown in Figure 4. On the lower side, the relative pressure is similar but with an opposite sign. It can be decomposed into a hydrostatic component P_h (obtained by vertical integration of the buoyancy force) and a component P_c imposed by the outer flow. Only the hydrostatic component (red in Figure 4) is present for a semi-infinite plate. The hydrostatic component leads to an upward lift force. For a finite plate, in contrast, the pressure from the outer flow is larger and has an opposite sign than the perturbation of the hydrostatic pressure. Thus, the net pressure (black in Figure 4) at the plate surface leads to a downward lift force. The imposed pressure diverges at the leading edge as $1/\sqrt{X}$, as predicted by the theory [3–5].

The numerical isotherms within the thermal boundary layer (Figure 3) are visually indistinguishable from the analytical isotherms according to [5] (not shown). The numerical and analytical [5] net pressure (solid and dashed black curves in Figure 4) agree very well, except in the vicinity of the leading edge. The slight difference between the numerical and analytical solutions is attributed to the weak flow separation, which is not considered in the analysis.

4.1 | Flow separation and non-uniqueness

A smaller channel height $B = 10$ is considered in this sub-section, and the Richardson number is gradually increased. As Ri increases beyond 0.05, the separation bubble at the lower side of the plate appreciably grows in size. In the range

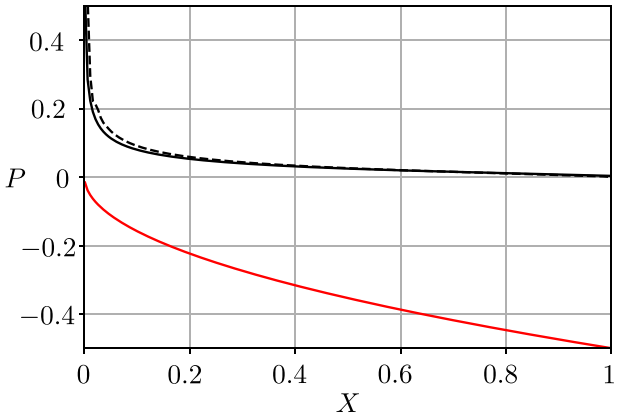

FIGURE 4 Distribution of the dimensionless relative pressure along the upper side of the plate. The hydrostatic component P_h is shown in red, while the black curves show the net pressure. The solid and dashed curves show the numerical result and the analytical solution of [5], respectively.

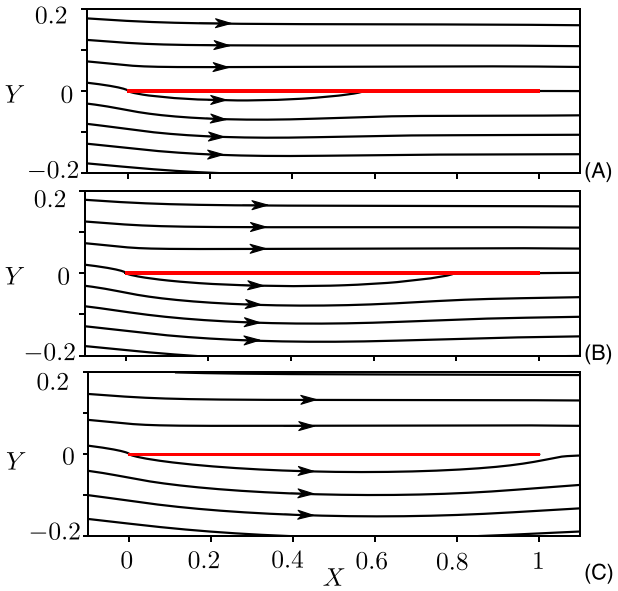

FIGURE 5 Co-existing numerical solutions for $B = 10$ and $\mathrm{Ri} = 0.083$, corresponding to the states (A), (B) and (C) indicated by dots in Figure 6.

$0.0754 < \mathrm{Ri} < 0.0838$, we find three co-existing solutions of the governing equations (2–8). These solutions, marked as (A), (B), and (C), are shown in Figure 5 for $\mathrm{Ri} = 0.083$. They differ by the length of the separation bubble, which reaches up to the trailing edge in Figure 5(C). The continuous evolution of the flow between these states upon the variation of Ri is resolved with the Pseudo Arc-Length Continuation method from the Library of Continuation Algorithms (LOCA) [8]. The total heat supply Q of the plate, quantified by the Nusselt number

$$\mathrm{Nu} = \frac{Q}{k\Delta T}, \tag{10}$$

where k is the heat conductivity of the fluid, is monitored as a function of the Richardson number. The resulting bifurcation diagram (Figure 6) shows a classical bistability of the states (A) and (C) with two turning points at $(\mathrm{Ri}, \mathrm{Nu}) = (0.0838, 38)$ and $(0.0754, 35.1)$. The solution (B) can be expected to be a separatrix between the basins of attraction of (A) and (C), as indicated by arrows in Figure 5. This results in a hysteresis of the flow upon a variation of the Richardson number. When Ri continuously increases from small values beyond 0.0838, the flow jumps from state (A) to (C), that is, the separation bubble attaches to the trailing edge. Afterward, if Ri decreases again, the separation bubble remains attached to the trailing edge until Ri drops below 0.0754. Then, the flow jumps back to the solution (A). It must be pointed out that the attracting

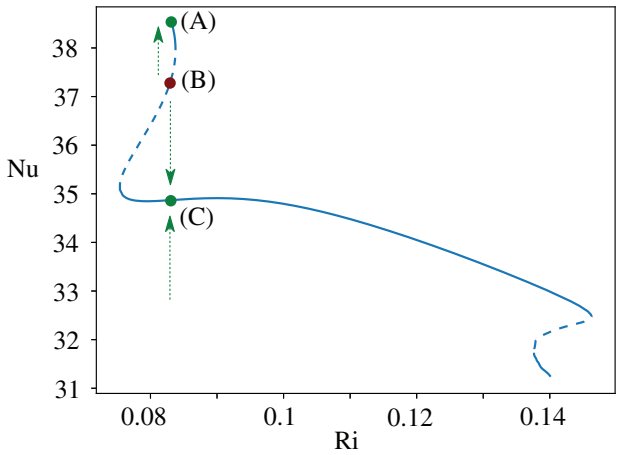

FIGURE 6 Dependence of the Nusselt number on the Richardson number for $B = 10$ obtained with the Pseudo Arc-Length Continuation method. The full and dashed parts of the blue curve indicate the expected attracting and repelling flow states. The dots indicate the solutions shown in Figure 5, and the arrows indicate the expected attraction of the states (A) and (C).

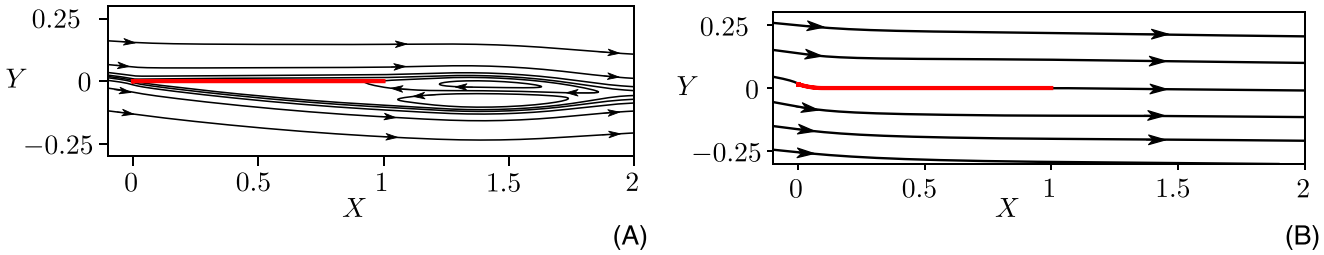

FIGURE 7 Flow around a flat plate (A) and around a plate with a bent leading edge with a tip angle $\alpha = 18°$ (B) for $B = 10$ and $\mathrm{Ri} = 0.143$. The contour levels of the stream function in (A) are distributed as a geometric series.

states (A) and (C) might still be unstable to oscillating perturbation. For Ri beyond 0.0838, the numerical solution (C) becomes unique until another bistability range $0.138 < \mathrm{Ri} < 0.146$ is reached.

4.2 | Separation control

Figure 7(A) shows the streamlines of the flow near the plate for $B = 10$ and $\mathrm{Ri} = 0.143$ corresponding to the upper part of the bifurcation curve in Figure 6. Two counter-rotating recirculation zones extend downstream beyond the trailing edge. One possibility to suppress the separation is to bend the leading edge. Thus, we bend the leading section of the plate of dimensionless length $L_b = 0.1$ with a constant radius of curvature and search for an optimal angle α between the leading edge and the horizontal plane $Y = \mathrm{const.}$. With the tip angle $\alpha = 18°$, the flow separation is completely avoided (Figure 7(B)). For larger Ri, a larger length L_b of the bent section would be needed to avoid the separation.

It should be pointed out that the rounded leading edge with a constant radius of curvature is not optimal. It is well known in the field of aerodynamics that an elliptical leading edge is more suitable for maintaining an attached flow. Our results for different parameters $\mathrm{Pr} = 1$, $\mathrm{Pe}_L = 20000$, $B = 10$ and $\mathrm{Ri} = 0.05$ indicate that in the case of a flat plate (Figure 8(A)), the flow separation can be suppressed by stretching the leading edge by a factor of 3 in the X-direction (Figure 8(B)).

5 | SUMMARY AND CONCLUSIONS

In this work, we find an excellent agreement between the numerically computed laminar flow around a finite heated plate in a channel and the corresponding analytical solution of [5] for large $\mathrm{Pe}_L = 400$, small $\mathrm{Pr} = 0.02$ and sufficiently low $\mathrm{Ri} = 0.05$. The hydrostatic pressure jump at the trailing edge and in the wake induces circulation in the outer potential

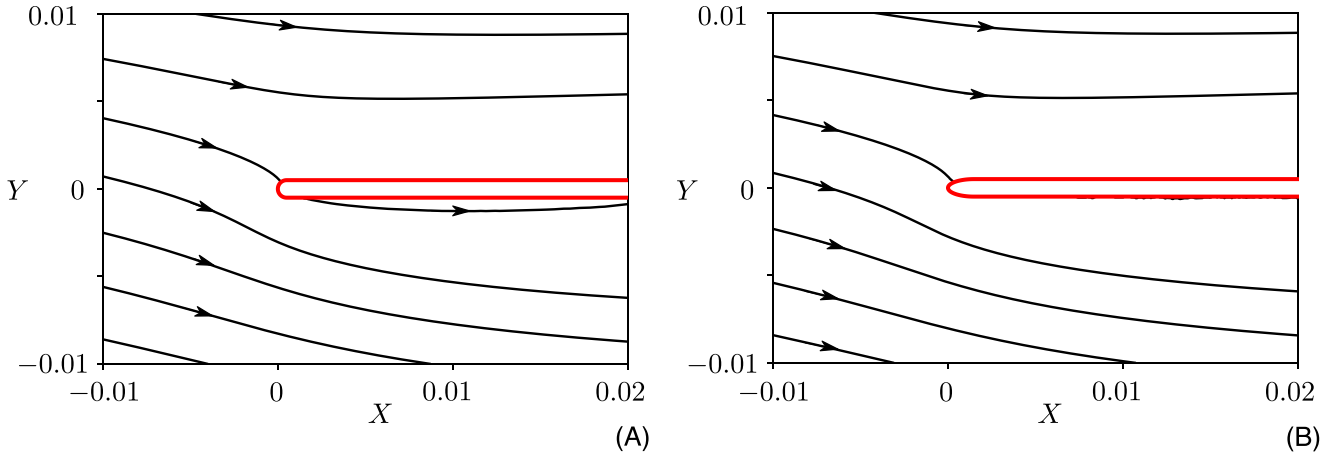

FIGURE 8 Flow near the cylindrical (A) and elliptical (B) leading edge with an aspect ratio of 3 (B) for a flat plate and Pr = 1, $Pe_L = 20000$, $B = 10$ and Ri = 0.05.

flow, leading to a lift force in the opposite direction compared to the buoyancy force. The flow tends to separate near the leading edge at the lower side of the plate. The size of the separation bubble is sensitive to the Richardson number. It grows significantly when Ri increases beyond 0.05, and thus, the numerical solution departs from the analytical one. In some intervals of the Richardson number, we find multiple (presumably bistable) steady two-dimensional flow states that differ by the length of the separation bubble. The flow separation can be postponed to higher values of Ri either by bending the leading edge or employing an elliptical rather than a cylindrical leading edge. The stability of the steady two-dimensional solution(s) presented here to time-dependent or three-dimensional perturbations remains an open question and is to be investigated as a planned extension of this work.

ACKNOWLEDGMENTS

The financial support of AIC Androsch International Management Consulting GmbH is gratefully acknowledged. The author thanks Prof. Wilhelm Schneider for a careful supervision of this project and Dr. Pierre-Emmanuel des Boscs for the implementation of the numerical Arc-Length Continuation algorithm.

ORCID

Lukas Babor https://orcid.org/0000-0002-7528-9326

REFERENCES

1. Blasius, H. (1908). Grenzschichten in Flüssigkeiten mit kleiner Reibung. *Zeitschrift für Angewandte Mathematik und Physik*, *56*, 1–37.
2. Schlichting, H., & Gersten, K. (2017). *Boundary-layer theory*. Springer-Verlag Berlin Heidelberg.
3. Schneider, W. (2000). In E. W. P. Hahne, W. Heidemann, & K. Spindler (Eds.), *Proceedings of the 3rd European thermal sciences conference*, (pp. 195–198). Edizioni ETS.
4. Schneider, W. (2005). Lift, thrust and heat transfer due to mixed convection flow past a horizontal plate of finite length. *Journal of Fluid Mechanics*, *529*, 51–69.
5. Müllner, M., & Schneider, W. (2010). Laminar mixed convection on a horizontal plate of finite length in a channel of finite width. *Heat and Mass Transfer*, *46*, 1097–1110.
6. Daeneke, T., Khoshmanesh, K., Mahmood, N., de Castro, I. A., Esrafilzadeh, D., Barrow, S. J., Dickey, M. D., & Kalantar-zadeh, K. (2018). Liquid metals: fundamentals and applications in chemistry. *Chemical Society Reviews*, *47*, 4073–4111.
7. Savić, L., & Steinrück, H. (2005). Mixed convection flow past a horizontal plate. *Theoretical and Applied Mechanics*, *32*, 1–19.
8. Salinger, A. G., Bou-Rabee, N. M., Pawlowski, R. P., Wilkes, E. D., Burroughs, E. A., Lehoucq, R. B., & Romero, L. A. (2002). *LOCA 1.0 Library of continuation algorithms: Theory and implementation manual*. Sandia National Laboratories.

How to cite this article: Babor, L. (2023). Numerical investigation of mixed convection flow over a heated horizontal plate of finite length. *Proceedings in Applied Mathematics and Mechanics*, *23,* e202300030. https://doi.org/10.1002/pamm.202300030